Fuel 371 (2024) 132014

Contents lists available at ScienceDirect

Fuel

journal homepage: www.elsevier.com/locate/fuel

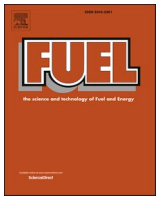

Experimental study on luminescence and thermal radiation characteristics of plasma assisted-biogas flames changing CO_2 dilution level

R. Paulauskas *, A. Jančauskas, E. Bykov, L. Vorotinskienė, K. Zakarauskas

Laboratory of Combustion Processes, Lithuanian Energy Institute, LT-44403 Kaunas, Lithuania

ARTICLE INFO

Keywords:
Biogas
Methane
CO_2
Plasma-assisted combustion
Emitters
Infrared
Radicals

ABSTRACT

This complex study focuses on the effect of CO_2 level (40–80 vol% of CO_2 in CH_4) in biogas to radiative flame characteristics and the influence of plasma assistance on them at different fuel equivalence ratios. During experimental studies, the spectrometric characteristics of the flame at different heights (0, 25, 50 mm) were analysed to investigate radiative properties by UV–VIS and MIR spectrometers and the influence of the plasma-assisted combustion.

The data obtained by infrared spectrometer indicated that the emission intensities of emitters are weakest at the ignition point of the mixture while the highest concentrations of emitters in the mid-IR range (1800–5800 nm) are formed in the upper part of the flame contrary to UV–VIS data. The increase of CO_2 content by 20 vol% in the mixtures led to decreased emission intensities up to 10 % for emitters in the range 2300 to 3500 nm and only 4–10 % for CO_2 emitter at 4450 nm.

The plasma assisted combustion improves combustion stability of mixtures with CO_2 dilution and ensures flammability of the mixture with 80 vol% of CO_2 in CH_4. In general, plasma leads to increased emission intensities of CO_2 and H_2O emitters at the burner nozzle from 13 to 11 % changing CO_2 dilution from 40 to 60 vol %. Approaching to leaner combustion regime, from $\phi = 0.71$ to 0.63, the plasma effect is more intense and the intensity of emitters increases by 18–22 % compared to the case without plasma assistance. Correlations between UV–VIS and MIR data were determined and predictions of the flame temperature were proposed as well.

1. Introduction

Thermal radiation plays a major role in heat transfer processes especially from the flames. This mode is important for energy-extensive industrial applications such as primary aluminium production, steel manufacturing, glass fabrication and other applications whose demand high temperatures for processing. For this reason, fossil fuels are used for decades due to fast energy demand response, high energy density and relatively clean combustion products considering the influence on the manufacturing product. But according to the newest EU ambitious on greenhouse gas (GHG) reduction targets, the energy sector, transportation, residential, and industrial sectors should be decarbonized replacing fossil fuels to alternative ones [1,2].

One of alternative fuels is biogas, which production via anaerobic digestion solves a lot of problems: biogenic waste utilization, reduction of methane emissions from lagoons, and substitute fossil fuel by biomethane [3,4]. Among the advantages there lays and disadvantages as the biogas composition is closely related to the available raw material and methane concentration in biogas could vary from 40 to 70 vol% with the remaining part of CO_2 [5]. High content of CO_2 affects the combustion process of biogas worsening the flame stability and flame creation, decreasing burning velocity [6–8]. As the flame temperature is affected by CO_2 presence, the combustion efficiency also drops resulting in higher CO emissions, though thermal NO formation is suppressed [6,7]. Also the high heat capacity of CO_2 reduces the reaction thickness of the flame [9]. According to [10], the mixture with higher CO_2 content than 50 % was not able to combust under normal conditions. Moreover, the flame luminosity and the flame structure in terms of volume and length were decreasing with increasing CO_2 content in the mixture. Machado et al. [11] determined that CO_2 dilution level up to 50 vol% in methane increases the radiative fraction, but soot suppression is observed at lower CO_2 dilution level, of 20 vol%. Mainly, these challenges are solved by implementing different methods as oxygen-enrichment [12], hydrogen [13] or ozone addition [14], non-thermal plasma application [15]. Among them, the plasma-assisted combustion gains high interest to improve the combustion process of alternative

* Corresponding author.
E-mail address: Rolandas.Paulauskas@lei.lt (R. Paulauskas).

https://doi.org/10.1016/j.fuel.2024.132014
Received 31 January 2024; Received in revised form 9 May 2024; Accepted 24 May 2024
Available online 28 May 2024

fuels such as biogas [16], low calorific value gases [17], ammonia [18] and etc. Ghabi et al. [19] examined the influence of pulse gliding arc parameters on non-premixed CH_4/CO_2 flame stability. Author determined that plasma-assisting improves the combustion quality, i.e., stability and efficiency. At a fixed plasma voltage (3–3.5 kV) and frequency (10 kHz) flame lift-off height depends on the CO_2 concentration, which determines the dilution effect, reaction temperature and the flame speed. The gliding arc effect was also investigated on blast furnace gas and the results showed that plasma assistance leads to extended flammability in terms of fuel equivalence ratio from 0.78 to 0.44, but with increasing flow from 40 to 120 l/min, the effect decreased from 44 to 7 % [20]. Also plasma-assisted combustion showed controversial results on soot formation in flames, which influences heat transfer by thermal radiation. According to [21], authors found that plasma-assisted flames leads to supressed soot, but based on findings by Qi et al. [22] soot suppression depends on the plasma discharge point in flames and power as at higher frequencies, enhanced generations of soot were observed.

Considering that during combustion of natural gas, thermal radiation is emitted in luminous and non-luminous spectral range by formed products (CO_2, H_2O, CO, soot) in flames [23], natural gas substitution with biogas could be challenging as the combustion of alternative fuels results in changes of combustion conditions, which in turn could reduce heat transfer by thermal radiation due to the reduced concentrations of emitters and changes in flame emissivity. Though, radiative characteristics of methane flames are well investigated [24–26] and the newest studies in the literature mainly focus on thermal radiation characteristics from fires [27,28], from non-premixed hydrocarbon flames [29] and also focus on intensification of thermal radiation [30,31]. However, there is a lack of works related to the spectral data of radiation from alternative fuels, especially assisted by non-thermal plasma, which could provide a better understanding of radiative heat transfer and gas radiation.

For these reasons, complex study focuses on the effect of CO_2 level (40–80 vol%) in biogas to radiative flame characteristics and the influence of plasma assistance on them at different fuel equivalence ratios. During experimental studies, the spectrometric characteristics of the flame at different heights (0, 25, 50 mm) were analysed to investigate radiative properties by UV–VIS and MIR spectrometers and the influence of the plasma-assisted combustion. The scientific novelty of the work consists on the extended knowledge of non-luminous emissions from biogas flames with varied content of CO_2, determined correlations between luminous (200–1100 nm range) and non-luminous (2000–5000 nm) radiation and predictions on flame temperature of plasma-assisted combustion.

2. Experimental setup and methodology

2.1. Experimental rig for low calorific value gases

The experimental combustion setup consists of the gas supply system, mixing chamber, plasma-assisted burner, combustion chamber, UV and NIR emission spectroscopy systems (see Fig. 1). Gases were supplied from cylinders and premixed in the mixing chamber with a length of 120 mm and an inner diameter of 35 mm. All flows of gases were controlled by high accuracy mass-flow controllers Brooks SLA 5800 operated by a controlling unit Brooks 0254. The combustion experiments were performed using the plasma-assisted burner. The burner was mounted in the combustion chamber with a diameter of 150 mm and a height of 600 mm made from quartz which ensured 90 % transmittance for the flame emission spectroscopy (see Fig. 1). The burner was designed to work under normal conditions and under plasma assistance, and consists of three main parts: a vane-swirler of 40° angle, a conical-shaped nozzle which also is an anode mounted on the coaxial rod and a metal exit tube which works as cathode. The gap between the electrodes was set to 2 mm. Both electrodes were made from construction metal S235. Below the conical-shaped nozzle, the vane-swirler made from a 3D printed ABS plastic and the plastic baffle were placed to distribute the flow and swirl the flow before ignition. A quartz tube with a diameter of 21 mm and a height of 30 mm was mounted at the top of the burner to prolong the residence time of the gas flow and increase the flame stability (Fig. 1). The plasma discharge of 120 kHz was generated using a plasma generator Redline Technologies G2000. For the characterization of the flame, two different spectrometer were used.

2.2. Luminous and non-luminous emission spectroscopy systems

During combustion experiments, the flame characterization was performed using two different spectrometers The luminous emission

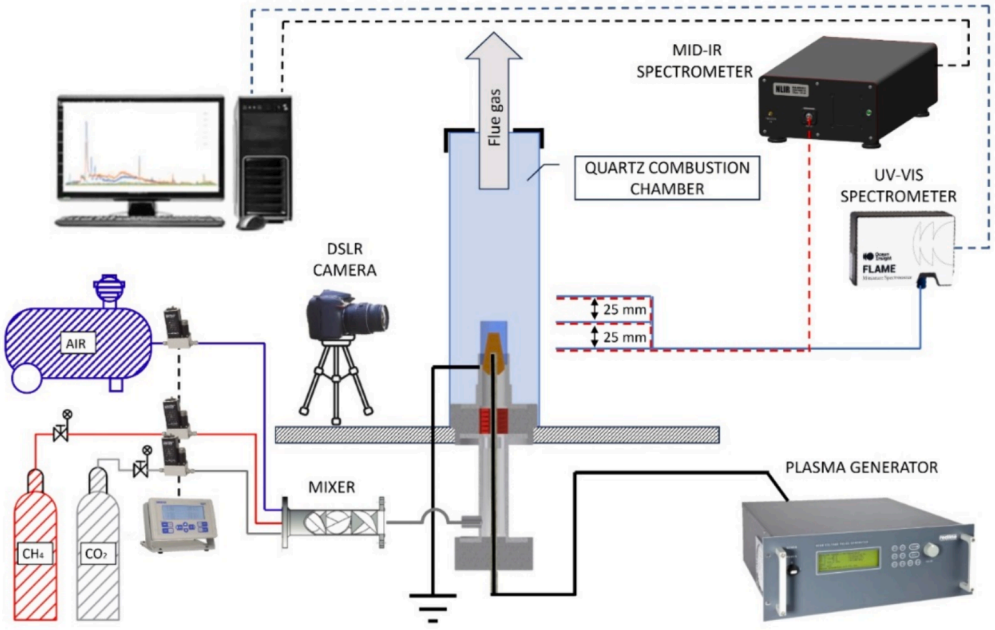

Fig. 1. Scheme of the experimental combustion rig.

spectra of the flame in the visible light and ultraviolet range was obtained using an Ocean Insight Flame S-XR1-ES spectrometer with range of 200–1025 nm coupled with 10° collimator. In further sections of the article, the luminous emission spectroscopy is indicated as the UV–VIS spectroscopy. The light from the flame was collected through a single-mode optic fiber (200–1100 nm) with fiber core size of 0.6 mm. The fiber tip was installed in an optical collimator and directed to the flame. Measurements were performed at different heights from the burner exit: 0 ± 0.05 mm, 25 ± 0.05 mm and 50 ± 0.05 mm. The spectrometer was controlled by Ocean Optics software and was set to average 30 scans with the integration time of 1 s to obtain the spectra for all tests.

The non-luminous emission spectroscopy was performed using a 2000–5000 nm spectrometer (NLIR S2050-400) with 400 kHz sampling option. In further sections of the article, the non-luminous spectroscopy performed by this spectrometer is indicated as the Mid-IR spectroscopy. The spectrometer was connected to a multi-mode optic fiber. The optic fiber has operating wavelength which covers the available range of the spectrometer (300–5500 nm) and the fiber was directed to the flame keeping the same distance as in the case of the flame emission spectroscopy above. The spectrometer was controlled using a NLIR NIR spectroscopy software and the spectra was obtained by averaging 30 scans with the integration time of 80 ms. The measurements were performed by changing a position of the fiber and collimator which corresponded to different heights from the burner (0 ± 0.05 mm, 25 ± 0.05 mm and 50 ± 0.05 mm) and were equal to these in the case of luminous emission spectroscopy for comparison purpose of results.

2.3. Procedure of combustion experiments

The experiments were performed using three compositions of synthetic biogases with different CO_2 dilution levels (40, 60 and 80 vol%). The composition of mixtures are presented in Table 1. The synthetic biogases were prepared supplying methane (CH_4 purity of 99.5 %) and carbon dioxide (CO_2 purity of 99.9 %) from cylinders to the mixing chamber. Compressed dry air was used as an oxidizer. The gas flows were controlled by mass flow controllers and flow values were set to maintain constant burner power (~1.32 kW) changing mixture composition and fuel to air ratio ϕ from 0.83 to 0.63 (see Table 1).

In order to investigate CO_2 dilution effect on radiative flame properties at different combustion conditions and to determine plasma influence on flame radiative properties, the combustion experiments were performed without plasma-assistance (identification – 0 kHz) and organizing the plasma-assisted combustion (120 kHz). The gliding arc discharge was formed using the plasma generator, which was set at 120 kHz and intermediate circuit voltage at 140 V. The burner configuration ensured that a vortex of flow spirals through the burner's inner chamber, progressing towards the smallest cross-sectional gap and the discharges are formed at the tightest space between the electrodes (0.9 mm) and is subsequently stretched along them by the momentum of the gas stream. The formed discharges move up the cone until the gap becomes too wide to maintain the discharge and is replaced by new one. This leads that the entire cross-section of the burner exit channel is enveloped by a lot plasma rotating plasma discharges, whose are called rotating gliding arcs and their length was 9.6 mm in the current configuration. In addition, to acquire current and voltage data at the discharge place, a high voltage probe Tektronix P6015A and a current measuring probe connected to a digital oscilloscope Rigol DS4014 were used. For the 120 kHz regime, the voltage reached up to 2015 V in peak with the peak current of 0.3185 A. The typical period for this regime was 8.35 μs, and the calculated average power was 170.22 W, which corresponded to ~ 13 % of the burner thermal power. More details on the experimental setup is presented in the previous work [17].

In both cases, flame emission spectroscopy was achieved using UV–VIS and Mid-IR spectrometers at different CO_2 dilution levels changing ϕ values. Also images of flames were obtained by a digital camera for determination of flame behaviour at different conditions. The imaging was performed with camera parameters set to the exposure time of 1/200 s and ISO 800.

2.4. Uncertainty analysis of measuring equipment

An uncertainty analysis of the experimental combustion procedures was performed. Sources of possible uncertainties were divided in three groups: the mixture preparation, UV and IR spectra measurement, and the uncertainty analysis was carried out according to parameters of used equipment and literature [32–34]. Below is presented Table 2 with results of possible uncertainty of applied measurement technique, details and uncertainty estimation in %. The use of the precise equipment ensured that the uncertainty level was below 2 %.

Table 2
Uncertainty analysis of experimental procedure.

Sources	Parameter	Purity/ Accuracy	Uncertainty
Mixture preparation	CH_4 gas in a cylinder	99.5 %	0.5 %
	CO_2 gas a cylinder	99 %	1 %
	MFC for CH4	99.82 %	0.18 %
	MFC for CO2	99.82 %	0.18 %
	MFC for air	99.80 %	0.20 %
	Sub-total		1.16 %
Measurement by flame emission spectroscopy	Resolution	1.69 nm	0.16 %
	SNR	250:1	0.4 %
	Sub-total	–	0.43 %
Measurement by infrared spectrometer	Resolution	6 cm^{-1}	0.32 %
	Noise	11 counts	0.25 %
	Sub-total		0.41
Total uncertainty of the UV measurement		1.24 %	
Total uncertainty of the IR measurement		1.23 %	
Uncertainty of temperature prediction via IR measurement		1.69 %	

Table 1
Combustion parameters.

Gas composition, vol %	LHV, MJ/ m^3	Frequency, kHz	Fuel to air ratio ϕ	CH_4 flow rate, l/ min	CO_2 flow rate, l/ min	Air flow rate, l/ min	Total flow, l/ min
CH_4-60/CO_2-40	21.60 ± 0.12	0, 120	0.63	2.200 ± 0.027	1.470 ± 0.054	33.52 ± 0.2	37.21 ± 0.21
			0.71			29.33 ± 0.2	33.02 ± 0.21
			0.83			25.14 ± 0.2	28.83 ± 0.21
CH_4-40/CO_2-60	14.40 ± 0.08	0, 120	0.63	2.200 ± 0.027	3.300 ± 0.054	33.52 ± 0.2	39.04 ± 0.21
			0.71			29.33 ± 0.2	34.85 ± 0.21
			0.83			25.14 ± 0.2	30.66 ± 0.21
CH_4-20/CO_2-80	7.20 ± 0.04	0, 120	0.63	2.200 ± 0.027	8.800 ± 0.079	33.52 ± 0.2	44.54 ± 0.22
			0.71			29.33 ± 0.2	40.35 ± 0.22
			0.83			25.14 ± 0.2	36.16 ± 0.22

3. Results and discussion

3.1. Flame behaviour analysis

Before the beginning of experimental investigations, the adiabatic flame temperature of selected biogas mixtures was estimated theoretically including heat loss ratio. Heat loss ratio was estimated based on biogas ignition temperature [35] and experimental data of flammability of mixtures with different CO_2 contents (Fig. 3), and set to 0.46. The flame temperature was achieved using an open source software tool Cantera [36] with GRI-Mech 3.0 [37] kinetic mechanism. The calculated flame temperature including uncertainty of mixture preparation is presented in Fig. 2.

The calculated adiabatic flame temperature with heat loss demonstrates relation with both fuel to air ratio φ and CO_2 dilution. For example, in a case of CH_4-60 vol%/CO_2-40 vol%, changing fuel to air ratio ϕ from 1.0 to 0.63, the flame temperature decreases by approximately 254 °C, though CO_2 dilution level increase has lower effect on the flame temperature. Increasing CO_2 content from 40 to 60 %, the flame temperature dropped by 93 °C. Similar tendencies were also obtained by Ghabi et al. [38]. Authors used equal methods to calculate adiabatic flame temperature of mixtures with CO_2 up to 50 vol%, but heat losses have not been taken into account as in this case.

The study examines the combustion of gas mixtures both in its regular combustion without plasma assistance (0 kHz) and with the application of gliding arc discharge (120 kHz). The tangible visualization of biogas flames diluted with different concentration of CO_2 varying fuel to air ratios ϕ is presented in Fig. 3. All images are aligned and the burner's elevation remains consistent. Visual analysis of obtained flame images shows that a lower part of flame kernel can be described with prominent light blue colour caused due to formed CH* radicals [20] while intense soot formation was only detected in the case of biogas with 60 % of CH_4 in CO_2 [19]. At ϕ = 0.83, yellowish spike above the swirled flame is observed and approaching to leaner combustion conditions, the yellowish flame intensity is decreasing till it is not detected. This occurs due to dilution by nitrogen as the thermal combustion power is maintained constant changing ϕ. N_2 increase in the mixture leads to decrease of the flame temperature and the concentration of soot precursors [11]. In the particular case, the adiabatic flame temperature decreases from 967 °C to 780 °C changing fuel to air ratio ϕ from 0.83 to 0.63. A CO_2 concentration increase in the combustible mixture also leads to the supress of the soot formation as yellowish flame was not observed in the mixtures of CH_4-40 vol% and CH_4-20 vol% in CO_2 (Fig. 2). According to Hoerlle et al. [39], CO_2 absorbs and emits thermal radiation and has higher thermal capacity compared to air leading to reduction of the flame temperature. This is also proved by the calculated flame temperature. An increase of CO_2 from 40 to 60 %, reduces the flame temperature from 895 °C to 735 °C, at ϕ = 0.83.

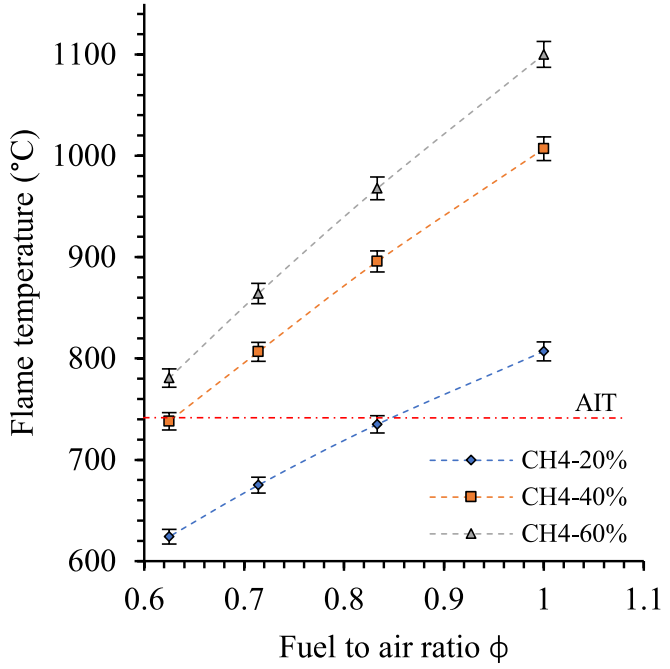

Fig. 2. The adiabatic flame temperature of different biogas mixtures versus ϕ.

During plasma-assisting combustion, the flame front shifts downwards to the source of the plasma discharge zone, and the reaction zone appears sooner. Besides, the plasma-assisted combustion leads to yellowish zone occurrence in the flames basically of all mixtures. Also, in the case of CH_4-40 % in CO_2, a more greyish flame at leaner combustion regime (ϕ = 0.63) is observed. It could be related to intense oxidation of carbon-containing radicals caused by plasma discharges while the flame temperature is considerably low and possibly CH* and soot formation is suppressed. According to [40], plasma discharges generate active species such as O*, OH*, NO*, N_2*, and OH* with ongoing partial methane and CO_2 reforming into CO and H_2 which leads to more intense oxidation of hydrocarbons and soot as well. Moreover, fuel oxidation reactions are enchased by thermal heat which is generated during the plasma discharge [41,42]. This phenomenon is more intense lowering CH_4 content to 20 vol% in CO_2. Besides, shifting to leaner combustion regime, the flame was formed deeper in the burner nozzle and greyish of the flame was intense. Considering the calculated flame temperature for this mixture without plasma assistance (around 700–750 °C), it is assumed that greyish flame was formed due to incomplete combustion with an intense oxidation of fuel in the plasma discharge zone.

3.2. Radiative characteristics of biogas flames

The obtained data by the UV–VIS spectrometer show that flame spectral emissions depend on a flame length and combustion conditions. Without plasma assistance (0 kHz), the highest emission intensities of formed main radicals (OH* at ~ 310 nm, CH* at ~ 431 nm and C_2* at ~ 508 nm) are observed at the burner exit (25 mm) regardless increasing CO_2 content from 40 to 60 vol% in CH_4 (Fig. 4). Though, the spectra of biogas flame with 40 vol% of CO_2 shows that the peaks of main radicals are also obtained at the nozzle (0 mm), but emission intensities are lower than ones at the burner exit (25 mm). It could be assumed that the emission intensities at 0 mm point indicates an ignition zone. Increasing the CO_2 content in the mixture, the flame is shifted up as the flame temperature decreases (Fig. 2) and the intensities obtained at the nozzle (0 mm) are considerably low indicating that the main reaction zone is relocated higher. Also a flame lift-off indicator could be considered CO_2* which is excited due oxidizing reactions and forms the continuum in a range of 250–700 nm and the peak plot correlates with intense oxidation of hydrocarbons (Fig. 4) [43]. However, the emission intensity of CO_2* is less related to the flame temperature comparing to the emission intensity of OH*, which is considered as a heat release marker [44]. For example, the higher CO_2 content (60 vol%) in the mixture leads to negligible area increase of the broad peak of CO_2* and the broad peak area corresponds to one obtained from biogas flames with 40 vol% of CO_2. Meanwhile OH* emission intensity drops by ~ 20 %. Moreover, an interesting group of emission intensity peaks were observed in the wavelength range from 850 to 1000 nm. In this range, the peaks were obtained at 50 mm from the burner nozzle, while emission intensities of OH*, CH* and C_2* were negligible. According to [45], the emission in this range is caused by vibrationally excited H_2O. Additionally, the intensity of these peaks at the burner exit (25 mm) correlates with flame temperature changes as increased CO_2 content in the mixture leads to a drop of intensity by 50 %. But, at the upper part of the flame (50 mm), intensities are near identical for both mixtures (Fig. 4). The changes in intensities of these peaks due to CO_2 dilution were observed by Ghabi et al. [19], but an explanation was not given.

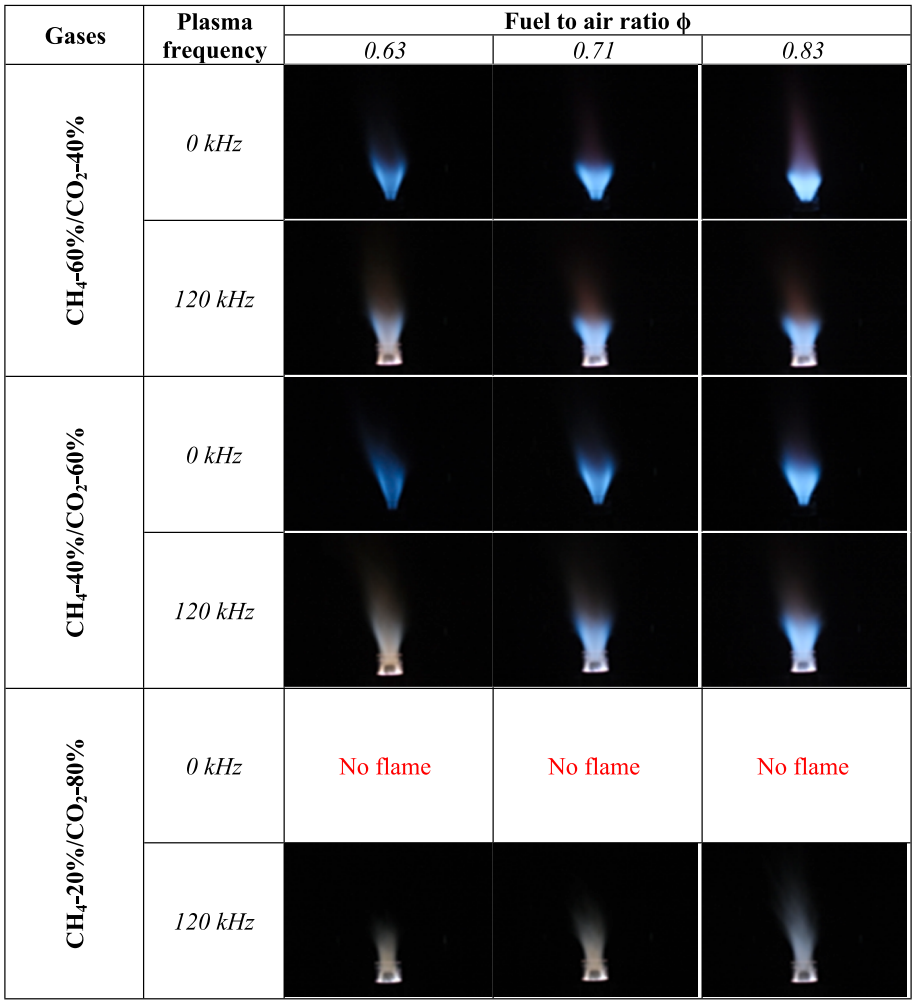

Fig. 3. Luminescence photographs of different composition biogas flames without plasma assistance (0 kHz) and with plasma (120 kHz) versus ϕ values.

During plasma-assisted combustion (120 kHz), more intense signals were obtained at the burner exit (0 mm) where the plasma discharge occurs. Based on the previous work [46], the plasma discharge results in a greater production of radical and excited species pool and depends on passed through gas composition. In this particular case, the highest peak was formed due excitation of OH* at the plasma discharge point (0 mm) and the intensity was higher than one at the burner exit (25 mm) for all mixtures (Fig. 4). Considering the presented results in [47,48], the increased OH* intensity could be related not only to CH_4/CO_2 reforming and more intense oxidation of fuel, but also to result of the electron impact and thermal effect at the plasma discharge point. Although, the continuum peak of CO_2* intensity occurred at the burner nozzle/plasma discharge point (0 mm) could be assumed as the indicator for more intense oxidation of the fuel molecules. Comparing combustion cases without (0 kHz) and with plasma (120 kHz), the continuum of CO_2* emission suggests that the flame is shifted down to the burner nozzle due to plasma discharge and combustion initiation is enhanced. Besides, the plasma discharge generated new excited species such as N_2* (C-B), NO*, CN* and O* in the flame [46]. Among them, O* plays important role for combustion enhancement [49] while the rest are responsible for more intense NOx formation [50]. Increasing the CO_2 content from 40 to 60 vol% in the mixture, the emission intensities of OH* and CO_2* becomes weaker at 0 mm while intensities of plasma produced species are near identical to the previous case (Fig. 4). Though the area of CO_2* is wider at the burner exit (25 mm) compared to the case without plasma discharge (0 kHz) and indicates that the oxidation of fuel is initiated closer to the burner nozzle. Moreover, the plasma-assisted combustion (120 kHz) of biogas with 60 % of CO_2 leads to near identical combustion characteristics as in the case of biogas combustion with 40 % of CO_2 without plasma assistance (0 kHz) (see Fig. 3 and Fig. 4). In the case of 80 vol% of CO_2 in the mixture, the combustion process was only available with plasma assistance, but overall emission intensities were considerably weak possibly due to low flame temperature. Considering that only OH* peak was clearly observed at the plasma discharge point (0 mm) and a lower intensity peak at the burner exit (25 mm), the ignition and combustion of the mixture was formed in the plasma discharge plot (Fig. 4). For better understanding of plasma influence on CO_2 diluted flames, the peak values of selected radicals (OH*, CH* and H_2O group) were extracted from the UV–VIS emissions spectra and arranged per height versus fuel to air ratio ϕ values and mixture compositions with and without plasma (see Fig. 5). Approaching to leaner combustion conditions (from $\phi = 0.83$ to 0.63), the peak values of OH*, CH* and H_2O group intensities decreased linearly (Fig. 5) and corresponded to the flame temperature (Fig. 2) especially at 25 mm position. Meanwhile, the increase of CO_2 content by 20 vol% in the mixture leads to the changed distribution of OH* and CH* emission intensity values per height. According to that, the flame shifts up OH* and CH* values at 0 mm point decrease few times while at 25 mm keep similar comparing to higher calorific value mixture. In case of plasma-assisted combustion, such evaluation from OH* and CH* emission intensity values is more complicated as OH* and CH* emission at 0 mm could be affected by electron impact and thermal effect due to plasma discharge. Comparing the observed emission distribution per the height, it is determined that excited H_2O group from flames has higher intensity at the top of the

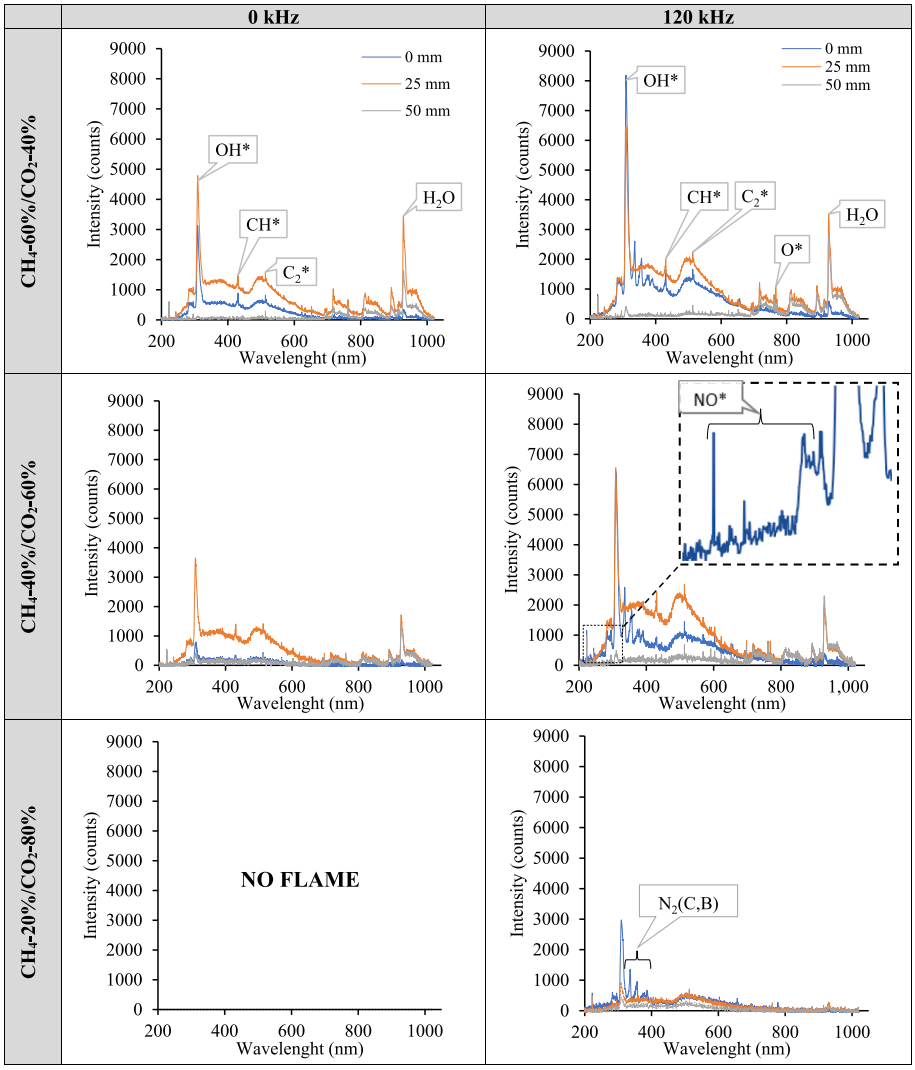

Fig. 4. Flame emission spectra of CH_4/CO_2 mixtures at fuel to air ratio $\phi = 0.83$.

flame (50 mm) instead at the burner nozzle (0 mm). Considered the flame structure increasing CO_2 content (Fig. 3), it could be assumed that the emission intensities of excited H_2O group is more related to the flame lift-off and indicate the heat release. Moreover, the intensities of this group are not affected by electron impact as in the case of OH* and CH* at 0 mm during plasma assisted combustion and could be considered for evaluation of combustion enhancement by plasma as the emission intensities of excited H_2O group is obtained higher, at 50 mm from the burner nozzle. Moreover, the obtained data by the Mid-IR spectrometer shows similar tendency.

The obtained IR spectra of biogas flames with different CO_2 dilution with and without plasma assistance are presented in Fig. 6. Extensive literature review reveals that main thermal radiation emitters are CO_2 and H_2O and they emits radiation at different wavelengths. In [51–53], it is suggested that CO_2 strongly emits at ~ 2000 nm and ~ 4400 nm wavelengths while water vapour in range of 1800–2000 nm and also overlaps with CO_2 at ~ 2700 nm. The newest works [54,55] indicate that intensity peak at 2500 nm wavelength is also caused by H_2O, and CO emission could be observed from 4900 nm. Analysing obtained IR spectra (Fig. 6), the most intensive peaks are located in the range from 2300 to 3500 nm and corresponds to water vapour (H_2O) and with overlapped carbon dioxide (H_2O + CO_2). Though, Henrion et al. [56] have observed that highest intensities are formed at wavelength of ~ 4300–4500 nm due to CO_2 emission and shows the best correlation with changing mixture composition. However it could be related to the use of a fused-silica cylinder, which has lowest transmission at ~ 2700 wavelength, for IR spectra observation [56], while there presented spectra were obtained directly from flames.

Analysing observed data per flame height it is coincident that the emission intensities of emitters are weakest at the ignition point of the mixture (0 mm) while the highest concentrations of emitters in the mid-IR range (1800–5800 nm) are formed in the upper part of the flame (at 50 mm) contrary to UV–VIS data. For example, a peak intensity at ~ 2500 nm is about 2 times higher at the flame top (50 mm) compared to the peak intensity at the ignition point (0 mm). Approaching to richer combustion regime, from $\phi = 0.63$ to 0.83, the intensity increase linearly as the flame temperature increase as well. This trend also corresponds to data presented by Lefebvre [57]. As well as it was expected, the increase of CO_2 content by 20 vol% in the mixtures led to decreased emission intensities up to 18 % and up to 10 % respectively at 25 mm and 50 mm especially for emitters in the range 2300 to 3500 nm and only 4–10 % for CO_2 emitter at wavelength of ~ 4450 nm (Fig. 6 (0 kHz)).

The mid-IR spectra obtained during plasma-assisted combustion (120 kHz) reveals that the plasma influence on thermal radiation emitters is negligible in the area of flame (Fig. 6 120 kHz). Though, the determined emission peak value distribution of main emitters per height reveals that plasma discharge leads to increased emission intensities of

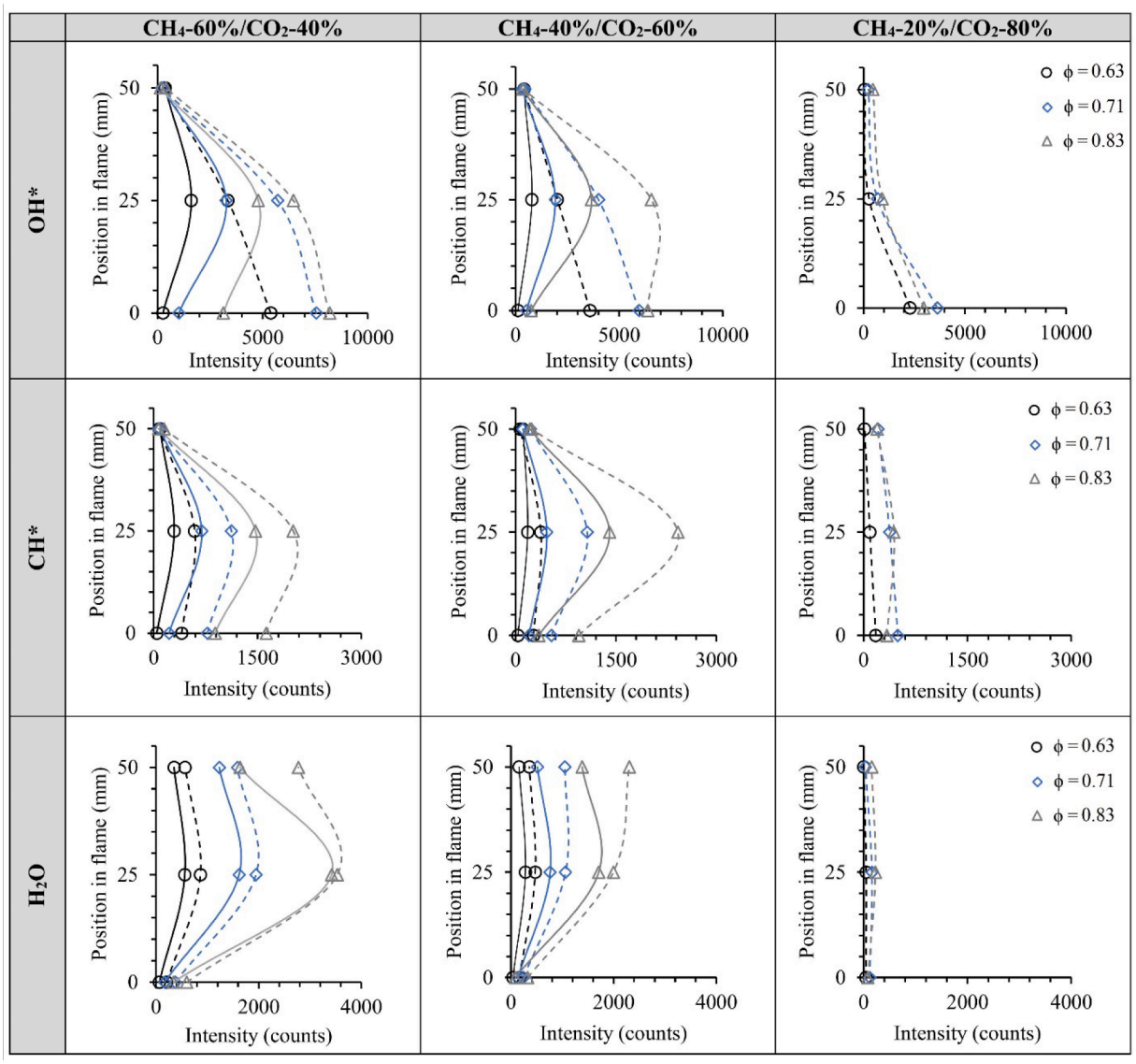

Fig. 5. Distribution of maximum intensities of excited radicals per height without (0 kHz – solid line) and with plasma (120 kHz – dash line).

these emitters at the burner nozzle, which also corresponds to the plasma discharge point (0 mm) from 13 to 11 % changing CO_2 dilution from 40 to 60 vol%. Approaching to leaner combustion regime, from ϕ = 0.71 to 0.63, the plasma effect is more intense and the intensity of emitters increases by 18–22 % compared to the case without plasma assistance. Moreover, the increase of the H_2O, H_2O + CO_2 and CO_2 emission intensities at the flame top (50 mm) are found in the lean-flame (at ϕ = 0.63) (Fig. 7). However, at richer combustion conditions (ϕ = 0.71 and 0.83) the plasma-assisted combustion leads to lower intensities of H_2O, H_2O + CO_2 and CO_2 emitters at the flame top (50 mm) compared to data without plasma assistance (0 kHz). Considering the obtained emissions intensities from the flame emission spectroscopy where plasma assistance leads to increased intensities of main radicals in the flame, the decrease in emission intensities of thermal radiation emitters at the measurement point of 50 mm could be caused by the changed flame position. Taking into account that determined emission intensities of radiative emitters is closely related to the temperature, the increased emissions at the plasma discharge point (0 mm) suggests the thermal effect caused by plasma which in turn shifts down the flame closer to the burner cone reducing the overall length of flame. Meanwhile at the leanest combustion regime (ϕ = 0.6) of biogas mixture with 60 vol% of CO_2, the plasma assistance plays significantly as intensities of IR emitters increase per flame and the increase level is the highest at 50 mm compared to the case without plasma assistance (Fig. 7). Besides, at the plasma discharge/ignition point (0 mm), the intensities of emitters are lower by 14 % compared to the identical case of mixture with 40 vol% of CO_2. According to the previous experiments [46], at this point the plasma discharge results in a higher kinetic effect by mixture reforming, for example decomposing part of CO_2 to CO, which in turn improves combustion characteristics while thermal effect is reduced. This plasma effect was also determined in the case of mixture with the highest CO_2 dilution level (80 vol% in CH_4), which is not combustible under normal conditions. The obtained intensities show that radiative properties of the plasma-assisted flame at ϕ = 0.83 and 0.71 become similar and even few percent's higher to the flames of higher calorific value mixture (60 vol% of CO_2 in CH_4) at leaner fuel condition (ϕ = 0.63) without plasma assistance. In overall, the obtained data show that more pronouncing effect of plasma assistance on the combustion enchantment is achieved at the leanest combustion conditions and at higher CO_2 levels resulting in more intense mixture reforming reactions [50].

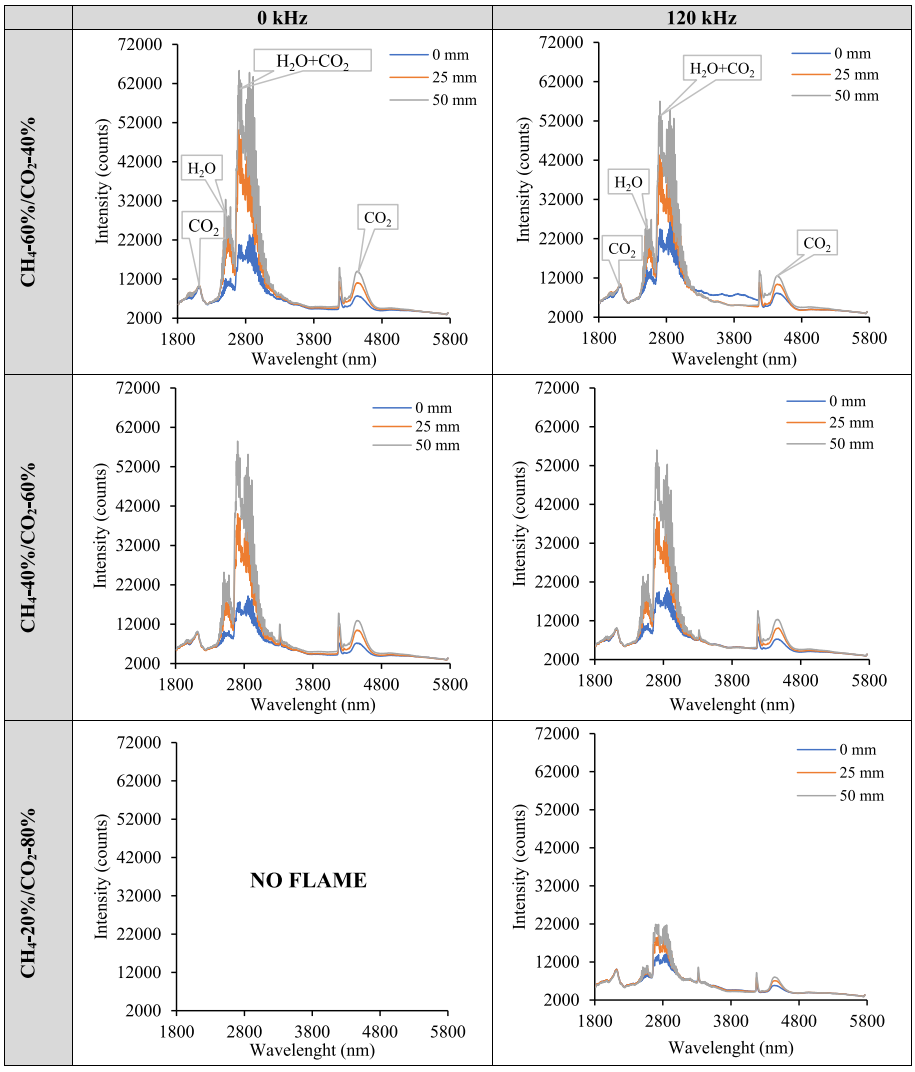

Fig. 6. Infrared radiation spectra from different CH_4/CO_2 flames at fuel to air ratio $\phi = 0.83$.

3.3. *Correlations between luminous and non-luminous emissions from CH_4/CO_2 flames*

For better understanding of the plasma effect on the flame characteristics at different heights, the dependency of the emission intensity of the excited H_2O group with OH*, and the dependency of CO_2 with H_2O radical group were estimated (Fig. 8). It was observed that luminous emission intensities linearly correlate with non-luminous emission intensities changing combustion characteristics, especially at measurement points of 0 mm and 25 mm. Taking into account that OH* is considered as a heat release marker [43,58], it clearly shows plasma effect (120 kHz) on OH* emission intensity increase at the ignition point (0 mm) compared to the case without plasma (0 kHz) and linearly correlates with H_2O emitter intensity changes as well. At the measurement height of 25 mm, the intensity correlation between H_2O and OH* has a positive relation as well, but the plasma effect leads to lower radiative properties of flames, especially increasing calorific value /decreasing CO_2 level in the mixture (Fig. 8). However, this trend reverses when the measurement height is 50 mm. As the intensity of OH* increases, the emission intensity of H_2O without plasma assistance (0 kHz) decreases, while it shows no clear relation in plasma assisted flames (120 kHz). This could be related to very low intensities of OH* at this point and also to the decreased flame lift-off due to plasma assistance as the H_2O emitter intensity also decreases compared to the case without plasma. Similar correlations were also determined of H_2O* emission intensity versus CO_2 intensity. Analysing data points obtained at 0, 25 and 50 mm, it was determined that H_2O* emission intensity linearly correlates with CO_2 emission intensity changing the combustion conditions and the positive plasma effect is only observed at poor combustion conditions (highest CO_2 level in the mixture) (Fig. 8). According to the obtained H_2O* graphs, the flame emission spectroscopy in the UV–VIS range could be used to foreseen radiative characteristics of the flames and also could be used to predict the flame temperature (Fig. 9). The CO_2 emission intensities were attributed to the calculated adiabatic flame temperature at the different CO_2 dilution level in the mixture and fuel to air ratio ϕ and the estimated pattern shows logarithmic correlation between emission intensity at ~ 4450 nm and the flame temperature. Analysing influence on combustion conditions, it was observed that increasing the CO_2 dilution level from 40 to 60 vol%, the CO_2 emission intensity drops from 11095 ± 136 to 10467 ± 129 counts at $\phi = 0.83$. Meanwhile at leaner fuel conditions ($\phi = 0.6$), the intensity drop is higher, from 8310 ± 102 to 6989 ± 86 counts but the changes in the flame temperature are similar in both cases, from 967 to 895 °C and from 780 to 733 °C, respectively. According to the estimated correlation, the flame temperature of plasma-assisted flames were evaluated. It was determined that plasma assistance leads to increased flame temperature by about 30 °C and that explains the flammability of mixture with high CO_2 level. Besides the evaluated plasma influence on

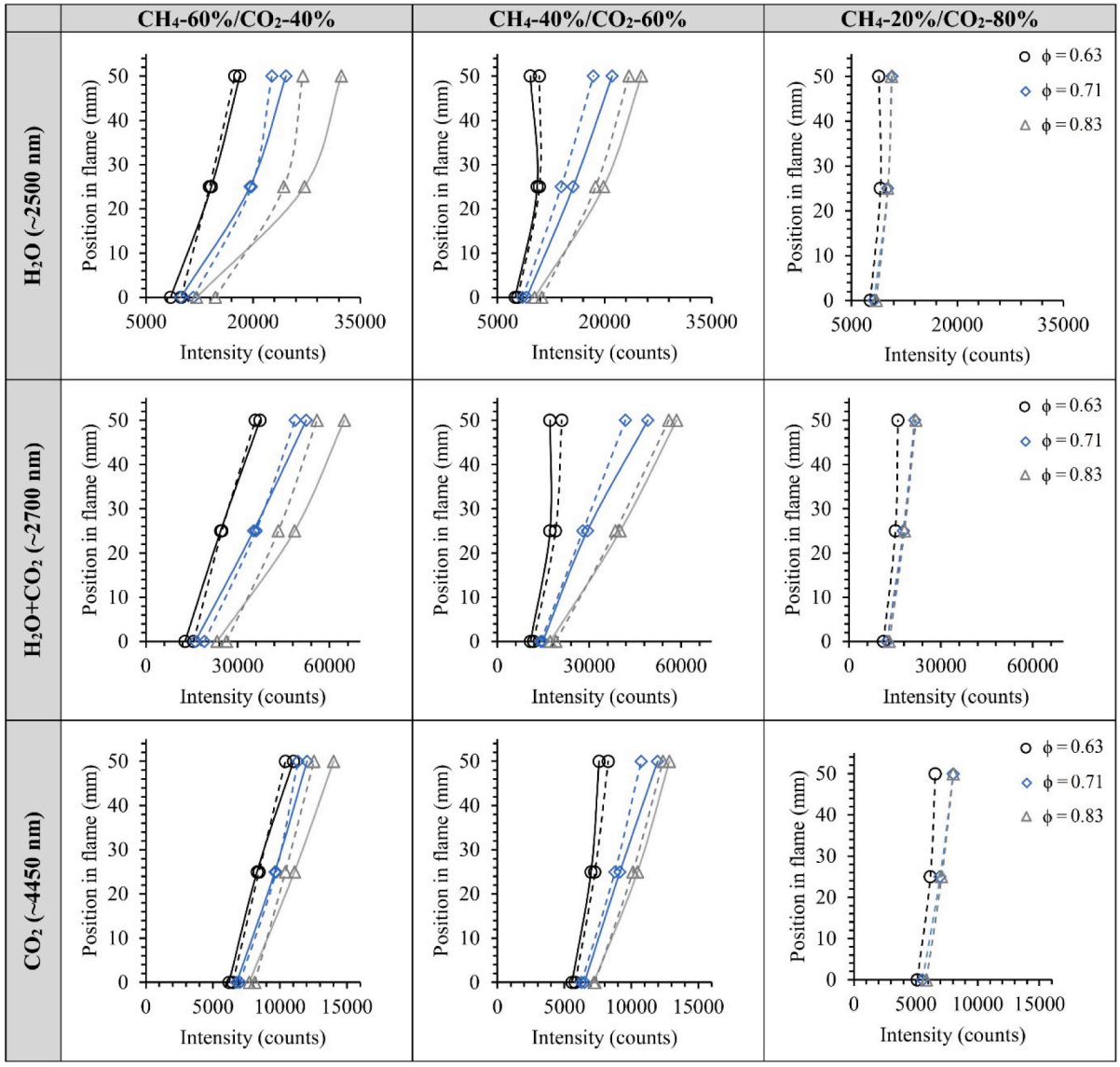

Fig. 7. Distribution of maximum IR intensities of emitters per height without (0 kHz) and with plasma (120 kHz).

the flame temperature corresponds to results presented by Ghabi et al. [16]. Moreover, the obtained results show that highest flame temperature increase is obtained at the leanest combustion conditions. It was also observed by Fei et al. [59], whose investigated the gliding arc discharge influence on the combustion process. Moreover, this trend as well corresponds with the data determined by flame emission spectroscopy in UV–VIS range (see Fig. 5).

Another pattern was found between H_2O^* emission intensity and the flame temperature, but the distribution of intensities are non-uniform scattered compared to the CO_2 emission intensity (Fig. 8). According to the estimated formula, the trend of plasma influence on the flame temperature is similar, but indicates lower impact as the flame temperature increase is predicted only about 10–18 °C. Besides, the determined values for mixtures with 80 vol% of CO_2 are considerably low and deceed CO ignition temperature revealing that H_2O^* emission intensity changes could be used only as indicator for flame temperature changes.

4. Conclusions

The experimental investigation was performed using a rotating gliding arc-assisted burner to determine the effect of CO_2 level in biogas on radiative flame characteristics and the influence of plasma assistance on them at different fuel equivalence ratios. The spectrometric characteristics of the flame (luminous and non-luminous emission) at different flame heights (0, 25, 50 mm) were determined.

The results reveal that the highest emission intensity of OH*, C_2^* and CH* are formed in the flame core (25 mm) and with increasing CO_2 level in the mixture emission intensity drops linearly. In the case of plasma assisted combustion, the highest emission intensities of these radicals are found at the plasma discharge point (0 mm). The plasma-assisted combustion of biogas with 60 % of CO_2 leads to near identical combustion characteristics as in the case of biogas combustion with 40 % of CO_2 without plasma assistance. Also the plasma assistance revealed significant effect on the flammability extension as stable combustion of mixture with 80 vol% of CO_2 was acquired. The peaks excited H_2O group in the wavelength range from 850 to 1000 nm were obtained at 50 mm from the burner nozzle, while emission intensities of OH*, CH* and C_2^* were negligible.

The data obtained by infrared spectrometer indicated that the emission intensities of emitters are weakest at the ignition point of the mixture (0 mm) while the highest concentrations of emitters in the mid-IR range (1800–5800 nm) are formed in the upper part of the flame (at

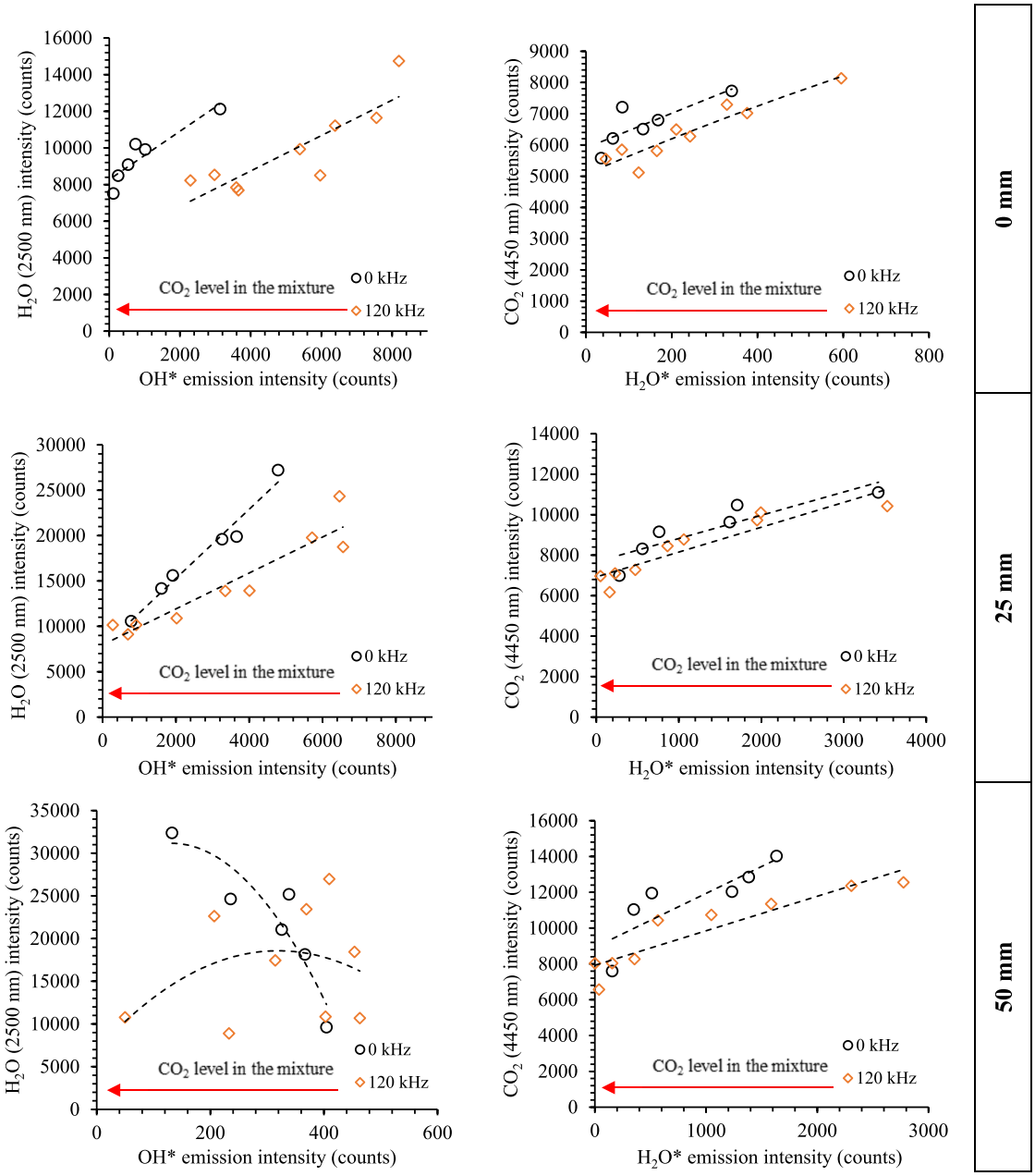

Fig. 8. Trends of OH* and H_2O* versus intensities of H_2O and CO_2 emitters at changing combustion conditions.

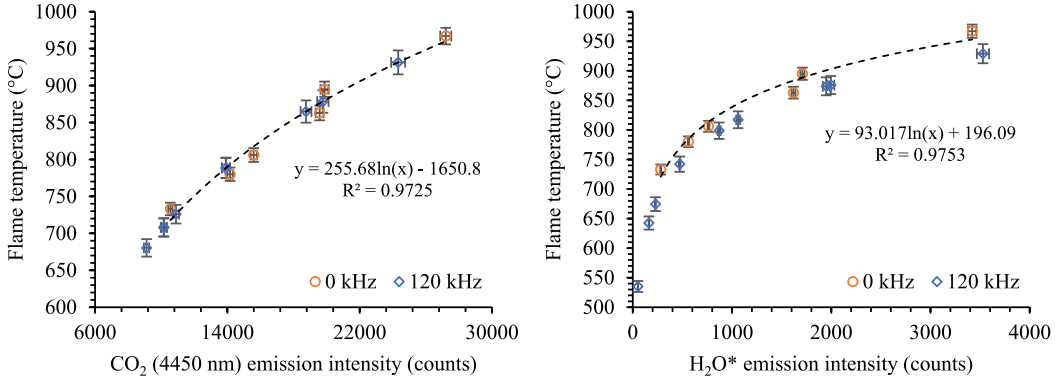

Fig. 9. CO_2 and H_2O* emission intensity in the flame core versus adiabatic flame temperature.

50 mm) contrary to UV–VIS data. The increase of CO_2 content by 20 vol % in the mixtures led to decreased emission intensities up to 18 % and up to 10 % respectively at 25 mm and 50 mm especially for emitters in the range 2300 to 3500 nm and only 4–10 % for CO_2 emitter at wavelength of ~ 4450 nm. The plasma assisted combustion leads to increased emission intensities of these emitters at the burner nozzle, which also corresponds to the plasma discharge point (0 mm) from 13 to 11 % changing CO_2 dilution from 40 to 60 vol%. Approaching to leaner combustion regime, from $\phi = 0.71$ to 0.63, the plasma effect is more intense and the intensity of emitters increases by 18–22 % compared to the case without plasma assistance. Moreover, the increase of the H_2O, $H_2O + CO_2$ and CO_2 emission intensities at the flame top (50 mm) are found in the lean-flame (at $\phi = 0.63$). However, at richer combustion conditions ($\phi = 0.71$ and 0.83) the plasma-assisted combustion leads to lower intensities of H_2O, $H_2O + CO_2$ and CO_2 emitters at the flame top (50 mm) compared to data without plasma assistance (0 kHz). It was assumed that it occurs due to decreased length of flame as during the plasma-assisted combustion the flame is moved closer to the burner cone.

It was determined that H_2O^* emission intensity in UV–VIS range linearly correlates with CO_2 emission intensity in MIR range changing the combustion conditions and the positive plasma effect is only observed at poor combustion conditions, but emissions intensity of CO_2 emitter correlates better with the adiabatic flame temperature.

Flame characterization using flame emission spectroscopy in the UV–VIS and MIR range could be promising technique to foreseen radiative characteristics of the flames and also for the flame temperature measurement. This is especially important in the plasma-assisted combustion, where electron impact influences the electronic devices or direct measurement devices as thermocouples. Flame temperature measurement in plasma-assisted flames could expand knowledge on plasma discharge influence on the flame and provide more details for numerical calculations. In future research, this technique coupled with heat flux measurement will be applied for zero carbon fuel (ammonia, hydrogen) plasma-assisted combustion to determine radiative characteristics changes without carbon footprint and to investigate possibilities of accurate temperature measurement via water vapour emission. Also to increase accuracy of the in-situ measurement for temperature of plasma-assisted flames, the experimental setup will be modified to apply the direct flame temperature measurement techniques of flames without plasma assistance and calibration will be applied for IR and temperature data correlations.

CRediT authorship contribution statement

R. Paulauskas: Writing – original draft, Visualization, Supervision, Resources, Project administration, Methodology, Funding acquisition, Formal analysis, Data curation, Conceptualization. **A. Jančauskas:** Writing – original draft, Visualization, Methodology, Investigation, Formal analysis, Data curation. **E. Bykov:** Writing – original draft, Methodology, Investigation, Formal analysis, Data curation. **L. Vorotinskienė:** Visualization, Investigation, Formal analysis. **K. Zakarauskas:** Methodology, Investigation, Formal analysis.

Declaration of competing interest

The authors declare that they have no known competing financial interests or personal relationships that could have appeared to influence the work reported in this paper.

Data availability

Data will be made available on request.

Acknowledgment

This project has received funding from the Research Council of Lithuania (LMTLT), agreement No S-MIP-23-116.

References

[1] Pichler M, Krenmayr N, Schneider E, Brand U. EU industrial policy: Between modernization and transformation of the automotive industry. Environ Innov Soc Transitions 2021;38:140–52. https://doi.org/10.1016/j.eist.2020.12.002.
[2] Slorach PC, Stamford L. Net zero in the heating sector: technological options and environmental sustainability from now to 2050. Energy Convers Manag 2021;230:113838. https://doi.org/10.1016/j.enconman.2021.113838.
[3] Brémond U, Bertrandias A, Steyer J-P, Bernet N, Carrere H. A vision of European biogas sector development towards 2030: trends and challenges. J Clean Prod 2021;287:125065. https://doi.org/10.1016/j.jclepro.2020.125065.
[4] Ullah Khan I, Hafiz Dzarfan Othman M, Hashim H, Matsuura T, Ismail AF, Rezaei-DashtArzhandi M, et al. Biogas as a renewable energy fuel – A review of biogas upgrading, utilisation and storage. Energy Convers Manag 2017;150:277–94. https://doi.org/10.1016/j.enconman.2017.08.035.
[5] Chen XY, Vinh-Thang H, Ramirez AA, Rodrigue D, Kaliaguine S. Membrane gas separation technologies for biogas upgrading. RSC Adv 2015;5:24399–448. https://doi.org/10.1039/C5RA00666J.
[6] Keramiotis C, Founti MA. An experimental investigation of stability and operation of a biogas fueled porous burner. Fuel 2013;103:278–84. https://doi.org/10.1016/j.fuel.2012.09.058.
[7] Watanabe H, Yamamoto J, Okazaki K. NOx formation and reduction mechanisms in staged O2/CO2 combustion. Combust Flame 2011;158:1255–63. https://doi.org/10.1016/j.combustflame.2010.11.006.
[8] Wei Z, Zhen H, Fu J, Leung C, Cheung C, Huang Z. Experimental and numerical study on the laminar burning velocity of hydrogen enriched biogas mixture. Int J Hydrogen Energy 2019;44:22240–9. https://doi.org/10.1016/j.ijhydene.2019.06.097.
[9] Yang J, Gong Y, Guo Q, Zhu H, He L, Yu G. Dilution effects of N2 and CO2 on flame structure and reaction characteristics in CH4/O2 flames. Exp Therm Fluid Sci 2019;108:16–24. https://doi.org/10.1016/j.expthermflusci.2019.06.003.
[10] Amez I, Castells B, Ortega MF, Llamas B, García-Torrent J. Experimental study of flame zones variations of biogas enriched with hydrogen. Int J Hydrogen Energy 2022;47:24212–22. https://doi.org/10.1016/j.ijhydene.2022.03.251.
[11] Machado IM, Pagot P, Pereira FM. Experimental study of radiative heat transfer from laminar non-premixed methane flames diluted with CO2 and N2. Int J Heat Mass Transf 2020;158:119984. https://doi.org/10.1016/j.ijheatmasstransfer.2020.119984.
[12] Yilmaz İ, Alabaş B, Taştan M, Tunç G. Effect of oxygen enrichment on the flame stability and emissions during biogas combustion: an experimental study. Fuel 2020;280:118703. https://doi.org/10.1016/j.fuel.2020.118703.
[13] Sivri I, Yilmaz H, Cam O, Yilmaz I. Combustion and emission characteristics of premixed biogas mixtures: an experimental study. Int J Hydrogen Energy 2021. https://doi.org/10.1016/j.ijhydene.2021.08.119.
[14] Ji S, Wang H, Shu M, Tian G, Lan X, Li M, et al. Investigation of combustion enhancement by ozone in a constant-volume combustion bomb. Energy Fuel 2019. https://doi.org/10.1021/acs.energyfuels.9b00775.
[15] Kong C, Li Z, Aldén M, Ehn A. Stabilization of a turbulent premixed flame by a plasma filament. Combust Flame 2019;208:79–85. https://doi.org/10.1016/j.combustflame.2019.07.002.
[16] Ghabi A, Darny T, Dozias S, Escot Bocanegra P, Pouvesle JM, Sarh B, et al. Effects of pulsed gliding arc plasma on non-premixed CH4/CO2– air flame stability. Therm Sci Eng Prog. 2023;40. https://doi.org/10.1016/j.tsep.2023.101764.
[17] Bykov E, Jančauskas A, Paulauskas R, Zakarauskas K, Striūgas N. Plasma assisted combustion of different biogas mixtures in low swirl burner. Fuel 2024;368:131602. https://doi.org/10.1016/j.fuel.2024.131602.
[18] Tang Y, Xie D, Shi B, Wang N, Li S. Flammability enhancement of swirling ammonia/air combustion using AC powered gliding arc discharges. Fuel 2022;313:122674. https://doi.org/10.1016/j.fuel.2021.122674.
[19] Ghabi A, Escot Bocanegra P, Sarh B, Dozias S, Robert E, Boushaki T. Experimental study of stability and pollutant emissions of turbulent biogas flames under microsecond pulsed plasma. Fuel 2023;353:129180. https://doi.org/10.1016/j.fuel.2023.129180.
[20] You B, Liu X, Yang R, Yan S, Mu Y, Zhang Z, et al. Experimental study of gliding arc plasma-assisted combustion in a blast furnace gas fuel model combustor: flame structures, extinction limits and combustion stability. Fuel 2022;322:124280. https://doi.org/10.1016/j.fuel.2022.124280.
[21] Cha M, Lee S, Kim K, Chung S. Soot suppression by nonthermal plasma in coflow jet diffusion flames using a dielectric barrier discharge. Combust Flame 2005;141:438–47. https://doi.org/10.1016/j.combustflame.2005.02.002.
[22] Qi D, Ying Y, Mei D, Tu X, Liu D. Soot characteristics from diffusion flames coupled with plasma. Fuel 2023;332:126126. https://doi.org/10.1016/j.fuel.2022.126126.
[23] Bourayou R, Vaillon R, Sacadura J-F. FTIR low resolution emission spectrometry of a laboratory-scale diffusion flame: experimental set-up. Exp Therm Fluid Sci 2002;26:181–7. https://doi.org/10.1016/S0894-1777(02)00125-5.
[24] Pouplin J, Collin A, Acem Z, Parent G, Boulet P, Vena P, et al. Study of a V-shape flame based on IR spectroscopy and IR imaging. J Phys Conf Ser 2016;676:012018. https://doi.org/10.1088/1742-6596/676/1/012018.

[25] Coelho PJ, Teerling OJ, Roekaerts D. Spectral radiative effects and turbulence/radiation interaction in a non-luminous turbulent jet diffusion flame. Combust Flame 2003;133:75–91. https://doi.org/10.1016/S0010-2180(02)00542-4.
[26] Plyler EK. (1955) Infrared flame spectra. Microchim Acta. 43:421–8. doi:10.1007/BF01235012.
[27] Quezada LA, Pagot PR, França FHR, Pereira FM. Experimental study of jet fire radiation and a new approach for optimizing the weighted multi-point source model by inverse methods. Fire Saf J 2020;113:102972. https://doi.org/10.1016/j.firesaf.2020.102972.
[28] Bordbar H, Alinejad F, Conley K, Ala-Nissila T, Hostikka S. Flame detection by heat from the infrared spectrum: optimization and sensitivity analysis. Fire Saf J 2022;133:103673. https://doi.org/10.1016/j.firesaf.2022.103673.
[29] Mazzei L, Puggelli S, Bertini D, Pampaloni D, Andreini A. Modelling soot production and thermal radiation for turbulent diffusion flames. EnergyProcedia 2017;126:826–33. https://doi.org/10.1016/j.egypro.2017.08.266.
[30] Shaddix CR, Williams TC. The effect of oxygen enrichment on soot formation and thermal radiation in turbulent, non-premixed methane flames. Proc Combust Inst 2017;36:4051–9. https://doi.org/10.1016/j.proci.2016.06.106.
[31] Irace PH, Gopan A, Axelbaum RL. An investigation of thermal radiation from laminar diffusion flames in a tri-coflow burner with central oxygen. Combust Flame 2022;242:112158. https://doi.org/10.1016/j.combustflame.2022.112158.
[32] da Jornada DH, ten Caten C, Pizzolato M. Guidance documents on measurement uncertainty: an overview and critical analysis. NCSLI Meas 2010;5:68–76. https://doi.org/10.1080/19315775.2010.11721507.
[33] Ronald H. Dieck. (2007) Measurement uncertainty : methods and applications. 4th rev.ed. ISA, North Carolina.
[34] Morrison FA. Uncertainty Analysis for Engineers and Scientists. Cambridge University Press; 2020. doi:10.1017/9781108777513.
[35] Mekonen EA, Mekonnen YT, Fatoba SO. Thermodynamic prediction of biogas production and combustion: the spontaneity and energy conversion efficiency from photosynthesis to combustion. Sci African 2023;21:e01776.
[36] Goodwin DG, Moffat HK, Cantera SRL. An object-oriented software toolkit for chemical kinetics, thermodynamics, and transport processes. Notes 2016. https://doi.org/10.5281/zenodo.170284.
[37] Smith GP, Golden DM, Frenklach M, Moriarty NW, Eiteneer B, Goldenberg M, et al. GRI-Mech 3.0. Http://WwwMeBerkeleyEdu/Gri_mech/ 2000. doi:10.1016/j.jinf.2014.08.011.
[38] Ghabi A, Boushaki T, Escot Bocanegra P, Robert E. Laminar burning velocity, adiabatic flame temperature, and pollutants of biogas/air mixture at various CO 2 concentrations and plasma assist. Combust Sci Technol 2023;195:1599–621. https://doi.org/10.1080/00102202.2023.2182202.
[39] Hoerlle CA, Pereira FM. Effects of CO2 addition on soot formation of ethylene non-premixed flames under oxygen enriched atmospheres. Combust Flame 2019;203:407–23. https://doi.org/10.1016/j.combustflame.2019.02.016.
[40] Ghabi A, Darny T, Dozias S, Escot Bocanegra P, Pouvesle J-M, Sarh B, et al. Effects of pulsed gliding arc plasma on non-premixed CH4/CO2– air flame stability. Therm Sci Eng Prog 2023;40:101764. https://doi.org/10.1016/j.tsep.2023.101764.
[41] Hwang N, Lee J, Lee DH, Song Y-H. Interactive phenomena of a rotating arc and a premixed CH4 flame. Plasma Chem Plasma Process 2012;32:187–200. https://doi.org/10.1007/s11090-012-9349-0.
[42] Gao J, Kong C, Zhu J, Ehn A, Hurtig T, Tang Y, et al. Visualization of instantaneous structure and dynamics of large-scale turbulent flames stabilized by a gliding arc discharge. Proc Combust Inst 2019;37:5629–36. https://doi.org/10.1016/j.proci.2018.06.030.
[43] He L, Guo Q, Gong Y, Wang F, Yu G. Investigation of OH* chemiluminescence and heat release in laminar methane–oxygen co-flow diffusion flames. Combust Flame 2019;201:12–22. https://doi.org/10.1016/j.combustflame.2018.12.009.
[44] Chen X, Wang Y, Zirwes T, Zhang F, Bockhorn H, Chen Z. Heat release rate markers for highly stretched premixed CH 4 /Air and CH 4 /H 2 /air flames. Energy Fuel 2021;35:13349–59. https://doi.org/10.1021/acs.energyfuels.1c02187.
[45] Schefer RW, Kulatilaka WD, Patterson BD, Settersten TB. Visible emission of hydrogen flames. Combust Flame 2009;156:1234–41. https://doi.org/10.1016/j.combustflame.2009.01.011.
[46] Bykov E, Striūgas N, Paulauskas R. Emission spectroscopy of CH4/CO2 mixtures processed in a non-thermal plasma augmented burner. Catalysts 2022;12:1540. https://doi.org/10.3390/catal12121540.
[47] Li T, Adamovich IV, Sutton JA. A burner platform for examining the effects of non-equilibrium plasmas on oxidation and combustion chemistry. Combust Sci Technol 2013;185:990–8. https://doi.org/10.1080/00102202.2013.769438.
[48] Hu Y, Tan J, Lv L, Li X. Investigations on quantitative measurement of heat release rate using chemiluminescence in premixed methane-air flames. Acta Astronaut 2019;164:277–86. https://doi.org/10.1016/j.actaastro.2019.07.019.
[49] Starik AM, Loukhovitski BI, Sharipov AS, Titova NS. Physics and chemistry of the influence of excited molecules on combustion enhancement. Philos Trans R Soc A Math Phys Eng Sci 2015;373:20140341. https://doi.org/10.1098/rsta.2014.0341.
[50] Paulauskas R, Martuzevičius D, Patel RB, Pelders JEH, Nijdam S, Dam NJ, et al. Biogas combustion with various oxidizers in a nanosecond DBD microplasma burner. Exp Therm Fluid Sci 2020;118:110166. https://doi.org/10.1016/j.expthermflusci.2020.110166.
[51] Ottesen DK, Stephenson DA. (1981) Fourier Transform Infrared (FTIR) Measurements In Sooting Flames. In: Sakai H, editor. 1981 Intl Conf Fourier Transform Infrared Spectrosc. Vol. 0289, p. 223–5. doi:10.1117/12.932176.
[52] Plyler EK, Humphreys CJ. Infrared emission spectra of flames. J Res Natl Bur Stand (1948) 1934;(40):449. https://doi.org/10.6028/jres.040.036.
[53] Faeth GM, Gore JP, Jeng S-M. Spectral and total radiation properties of turbulent carbon monoxide/air diffusion flames. AIAA J 1987;25:339–45. https://doi.org/10.2514/3.9627.
[54] Henrion L, Sick V, Haworth DC. A detailed experimental and modeling comparison of molecular radiative heat loss in a spark-ignition engine. Combust Flame 2022;241:112083. https://doi.org/10.1016/j.combustflame.2022.112083.
[55] Parent G, Acem Z, Lechêne S, Boulet P. Measurement of infrared radiation emitted by the flame of a vegetation fire. Int J Therm Sci 2010;49:555–62. https://doi.org/10.1016/j.ijthermalsci.2009.08.006.
[56] Henrion L, Gross MC, Fernandez SF, Paul C, Kazmouz S, Sick V, et al. Characterization of radiative heat transfer in a spark-ignition engine through high-speed experiments and simulations. OilGasSci Technol – Rev d'IFP Energies Nouv 2019;74:61. https://doi.org/10.2516/ogst/2019030.
[57] Lefebvre AH. Radiation from flames in gas turbines and rocket engines. Symp Combust 1969;12:1247–53. https://doi.org/10.1016/S0082-0784(69)80501-1.
[58] Doan NA, Swaminathan N. Analysis of markers for combustion mode and heat release in MILD combustion using DNS data. Combust Sci Technol 2019;191:1059–78. https://doi.org/10.1080/00102202.2019.1610746.
[59] Fei L, Zhao B-B, Chen Y, He L-M, Zhao Z-C, Lei J-P. Rotating gliding arc discharge plasma-assisted combustion from ignition hole. Exp Therm Fluid Sci 2021;129:110473. https://doi.org/10.1016/j.expthermflusci.2021.110473.